Tellus (1996), 48B, 000–000
Printed in UK – all rights reserved

TELLUS
ISSN 0280–6509

Spatial and temporal variability of ^{7}Be surface concentrations

By DOROTHY M. KOCH[1,*] and MICHAEL E. MANN, *Department of Geology & Geophysics, P.O. Box 208109, Yale University, New Haven, CT065120–8109, USA*

(Manuscript received 24 April 1995; in final form 15 September 1995)

ABSTRACT

^{7}Be ($t_{1/2}$ = 53 days) is generated by cosmic rays in the upper troposphere and stratosphere, and is a tracer of downward aerosol transport. We apply a singular value decomposition (SVD)-based technique, which simultaneously determines patterns of significant spatial and temporal variability, to ^{7}Be surface concentration data records that are 22 years long, from 19 locations distributed globally. Significant variability occurs on time scales corresponding to the solar cycle (≈11 years), El Niño/Southern Oscillation (≈2–3 years), an annual cycle, and a semi-annual cycle. The phase of the solar cycle signal varies little globally, except at the south pole, where low magnetic shielding may permit direct penetration of solar particles during times of high solar activity. The spatial variability of the phase of the ENSO signal corresponds with the effects of observed rainfall anomalies during ENSO. The phases of the annual and semi-annual signals depend upon the spatial distribution of vertical transport and precipitation. The temporal variabilities, or modes, corresponding to these signals sum together to form a variety of annual ^{7}Be cyclicities at different locations. We compare reconstructions of the time series based on the SVD analysis with the observed time series at 6 locations. The 4 modes explain between 19% and 47% of the monthly variance at these 6 sites. We show how various locations are affected by differing relative amounts and phases of the 4 signals. We also calculated the spatial variability of the annual cycle phase from a larger data set, by fitting a sinusoid to the average annual cycles at the sites. The agreement between the SVD and the sine-fitting results serves to validate both approaches.

1. Introduction

A variety of atmospheric processes affect the surface air concentration of ^{7}Be, a natural radionuclide ($t_{1/2}$ = 53 days) that is produced in the stratosphere and upper troposphere and is carried on aerosols (Feely et al., 1988). Although the timing and magnitude of their effects differ with location, the 2 processes that have the greatest short-term influences on ^{7}Be in surface air are precipitation, which scavenges the carrier aerosols, and downward transport, such as that associated with convective subsidence or the descending limbs of the Hadley circulation. Analysis of the spatial and temporal variation of ^{7}Be allows assessment of the influence of these processes on tropospheric aerosols.

On longer time scales, ^{7}Be concentration varies as its production is modulated by the (≈11 year) solar cycle. High solar activity deflects cosmic rays away from the solar system and the cosmogenic radionuclide production decreases (e.g., Lal and Peters, 1967; O'Brien et al., 1991). This phenomenon has been studied extensively for long-lived cosmogenic radionuclides such as ^{10}Be ($t_{1/2}$ = 1.5×10^{6} years) and ^{14}C ($t_{1/2}$ = 5730 years). Because of its 53-day half-life, the ^{7}Be inventory tracks

* Corresponding author.
[1] Present address: Dorothy Koch, NASA GISS/Columbia Univ., 2880 Broadway, New York, NY, 10025, U.S.A. email address: koch@thebes.giss.nasa.gov.

solar variability relatively closely and therefore provides more detailed information about short-term variations in solar activity as it affects cosmogenic radionuclide production. The anti-correlation between ^{7}Be and solar activity has been noted in short records (O'Brien et al., 1991; Larsen, 1993) and in longer records from Germany (Hötzl et al., 1991).

In an effort to assess the spatial and temporal variability of the solar cycle, transport, and scavenging effects on ^{7}Be concentrations, we use a method based on singular value decomposition (SVD) in the spectral domain. The phase of the signals is permitted to vary spatially, so that the strength of a given signal will not be compromised by the tendency for identical physical processes to be active during different seasons at different locations. Thus, for example, a strong annual cycle appears in the analysis even though it is generally 180° out of phase in the northern and southern hemispheres (Feely et al., 1988). The SVD analysis is most effective if the data records provide good global coverage and are at least twice as long as the period of the longest process under investigation. The available ^{7}Be data fulfill these requirements fairly well. The Environmental Measurements Laboratory, the Physikalisch Technische Bundesanstalt, and other laboratories established to monitor nuclear fallout have been measuring ^{7}Be air concentrations for over 2 decades. As a result, there are 16 widely distributed records, mostly in the western hemisphere (Fig. 3), which are longer than 20 years (Feely et al., 1981, 1985, 1988; Larsen and Sanderson, 1990, 1991; Larsen, unpublished data; Kolb, 1992).

2. The SVD method and results

We performed 2 experiments, the first (case "A") made use of 13 years of data from 19 sites, and the second ("B") included 22 years of data from 15 sites. The 1st case provides better spatial coverage and the 2nd greater temporal duration. We present a brief description of the SVD technique and refer to previous publications (Mann and Park, 1994; Mann et al., 1995) for further detail.

First the mean values are removed from each ^{7}Be series and each series is normalized by its standard deviation $\sigma(m)$. We take the tapered Fourier transforms of the mth normalized data series $x_n^{(m)}$ ($n=1,\ldots N$ months):

$$Y_k^{(m)}(f)=\sum_{n=1}^{N} w_n^{(k)} x_n^{(m)} e^{i2\pi f n\Delta t}, \qquad (1)$$

where $\Delta t=1$ month is the sampling interval and $\{w_n^{(k)}\}_{n=1}^{N}$ is the kth member in an orthogonal sequence of Slepian tapers, $k=1,\ldots K$ (Thomson, 1982; Lees and Park, 1995; Percival and Walden, 1993). $K=3$ is chosen to optimize the tradeoff between variance and spectral resolution. The matrix A is constructed, and is decomposed with a complex-valued SVD into K orthonormal left-eigenvectors u_k and right-eigenvectors v_k, scaled by an eigenvalue λ_k:

$$A(f)=\begin{bmatrix} Y_1^{(1)} & Y_2^{(1)} & \ldots & Y_K^{(1)} \\ Y_1^{(2)} & Y_2^{(2)} & \ldots & Y_K^{(2)} \\ \vdots & & & \\ Y_1^{(M)} & Y_2^{(M)} & \ldots & Y_K^{(M)} \end{bmatrix}$$

$$=U^{\dagger}\Lambda V=\sum_{k=1}^{K}\lambda_k(f)u_k(f)\otimes v_k^{*}(f). \qquad (2)$$

The V_k are complex-valued K-vectors (empirical orthogonal functions, or EOFs, in the spectral domain) which can be inverted to obtain the time-dependent, slowly varying envelope that modulates the carrier oscillation. Thus, the amplitude of the mode corresponding to the carrier frequency may

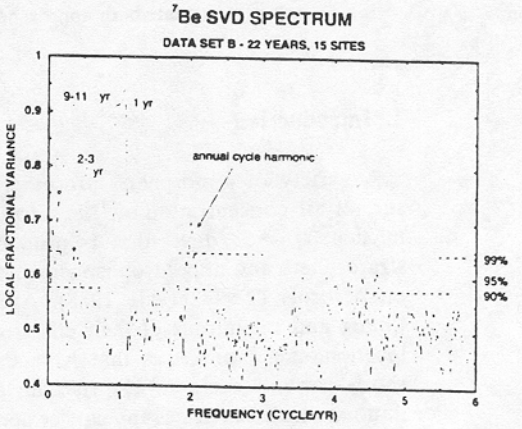

Fig. 1. SVD spectrum showing significant fractional variance at frequencies corresponding to $t\approx 11$, 2.5, 1, and 0.5 years. Dashed lines are 90% 95% and 99% significance levels, based on resampling (see text). Due to its proximity to the secular trend, the significance of the 11-year signal is about 92%.

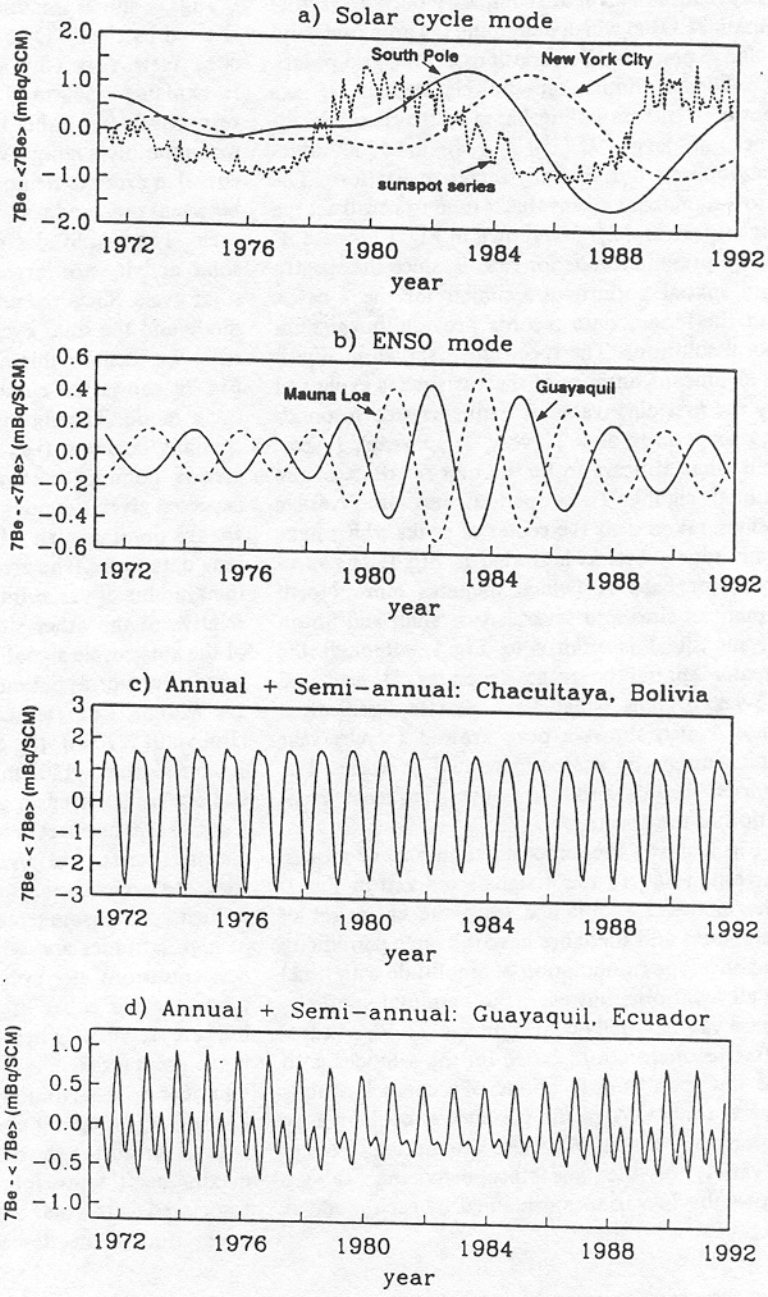

Fig. 2. Temporal modes shown for various locations. The units are concentration (mBq/m^3 at standard temperature and pressure) minus the mean value at each site. (a) The 11-year mode at New York City and the South Pole, shown with the normalized Wolf sunspot series (monthly averages). (b) The ENSO mode at Mauna Loa, Hawaii and Guayaquil, Ecuador. (c,d) The annual+semi-annual modes at Chacultaya, Bolivia and Guayaquil, Ecuador respectively.

vary in time. The u_k are complex-valued M-vectors (spatial EOFs) which determine the amplitude and relative phase of ^{7}Be variations among grid points. Confidence limits on the eigenvalues λ_k are obtained by resampling, based on the chance incidence of large $\lambda_k^2/(\lambda_1^2+\lambda_2^2+\lambda_3^2)$ in 1000 time-randomized but spatially intact realizations. The most significant eigenvalue is used to construct the eigenspectrum, $\lambda_1^2/\Sigma\lambda_k^2$, shown in Fig. 1 for case B.

We present results for case B, since the spectra and spatial patterns are similar for the 2 cases, but the longer data records provide longer temporal solutions. The spectrum is shown in Fig. 1. A significant amount of the variance is explained by the first eigenvalue at frequencies corresponding to periods of $\approx$11 year, $\approx$2.5 years, 1 year, and what appears to be the first overtone of the annual signal. These periodicities are average values, taken near the center of peaks which have a broader range, as indicated in Fig. 1. The spectrum for case A (which includes more North American sites and several Australian and South Pacific sites) is similar to Fig. 1, although the greater spatial coverage generates 11-year and 2.5-year signals which have greater significance. Case A also shows a peak around 3 cycles/year which might be a second annual overtone. The shorter records produce poorer frequency resolution in the spectrum.

Fig. 2 shows the temporal solutions, or modes, corresponding to the 4 signals marked in Fig. 1. The modes are obtained from the entire set of data series and therefore have the same periodicity and envelope (modulation of amplitude with time) at all locations; however, the amplitude and the phase vary spatially (shown in Fig. 3). Fig. 4 compares reconstructions based on the 4 modes with the raw data at 6 locations. We chose locations where a large % of the variance is explained by at least one mode, while also attempting to select a variety of ^{7}Be variability behaviors. Table 1 shows the % variance explained by each mode at each of these 6 sites.

Fig. 2a shows the time-dependent 11-year mode derived by the SVD as it appears at 2 contrasting sites, New York City and the South Pole, where it explains 25% and 14% of the variability, respectively (see Table 1). We also plot the normalized monthly-average Wolf sunspot series (dashed curve) in order to demonstrate the anti-correlation between the mode at New York and the solar cycle. The amplitudes of both the mode and the solar activity are largest during the most recent solar cycle. Since the anti-correlation between the mode and the solar cycle is observed at nearly all sites, we identify this as the "solar cycle" mode. Fig. 3a shows the spatial variability of the solar cycle mode. The figure shows that the mode is spatially coherent (i.e., temporally in phase, with arrows pointing eastward), as much as can be expected given the poor temporal resolution, since we are obtaining an 11-year signal from 22-year long data series. The arrow sizes in Fig. 3a indicate the amount of variability explained by this mode, relative to the other sites. Although the strength of the solar cycle signal varies, altitude or latitude trends are not apparent. The high elevation sites are Mauna Loa (Hawaii) (3400 m), Chacultaya (Bolivia) (5220 m), the South Pole (2800 m), and Rexburg, Idaho (1502 m). Although the solar cycle has a significant effect at all of these sites except Chacultaya, its effect is nearly as large at the lower elevation sites. Lal and Peters (1967) suggested that the solar cycle should have the strongest influence on cosmogenic radionuclide production at high latitudes and within the stratosphere. ^{7}Be concentrations do not, however, appear to be more affected either at high latitudes or in mid-latitude regions, where maximum stratospheric input is expected. The South Pole record shows a unique response to the solar cycle (Fig. 2a; see also Fig. 4f). Highest concentrations at the South Pole occur during the descending limb of the solar maximum. It is possible that low-energy particles associated with solar flares, which are most frequent during the descending limb of the solar

Fig. 3. Spatial variability of modes. Arrow direction indicates phase shift of the mode relative to the other sites (in the clockwise direction for (a) and (b)). Arrow size indicates relative amount of variability explained by the mode. Sites are located at arrow tails, except for the South Pole station which is at 90°S. (a) Spatial pattern for the "solar cycle". Comparison of Figs. 2a and 3a shows that an eastward pointing arrow corresponds to the mode maximum. (b) Spatial pattern for "ENSO". Black and gray arrows are in regions expected to have increased and decreased scavenging of ^{7}Be respectively. Remaining arrows are outlined. (c,d) Spatial pattern for the annual and semi-annual cycles. The arrows are oriented to indicate the maximum concentrations according to the illustrated scale.

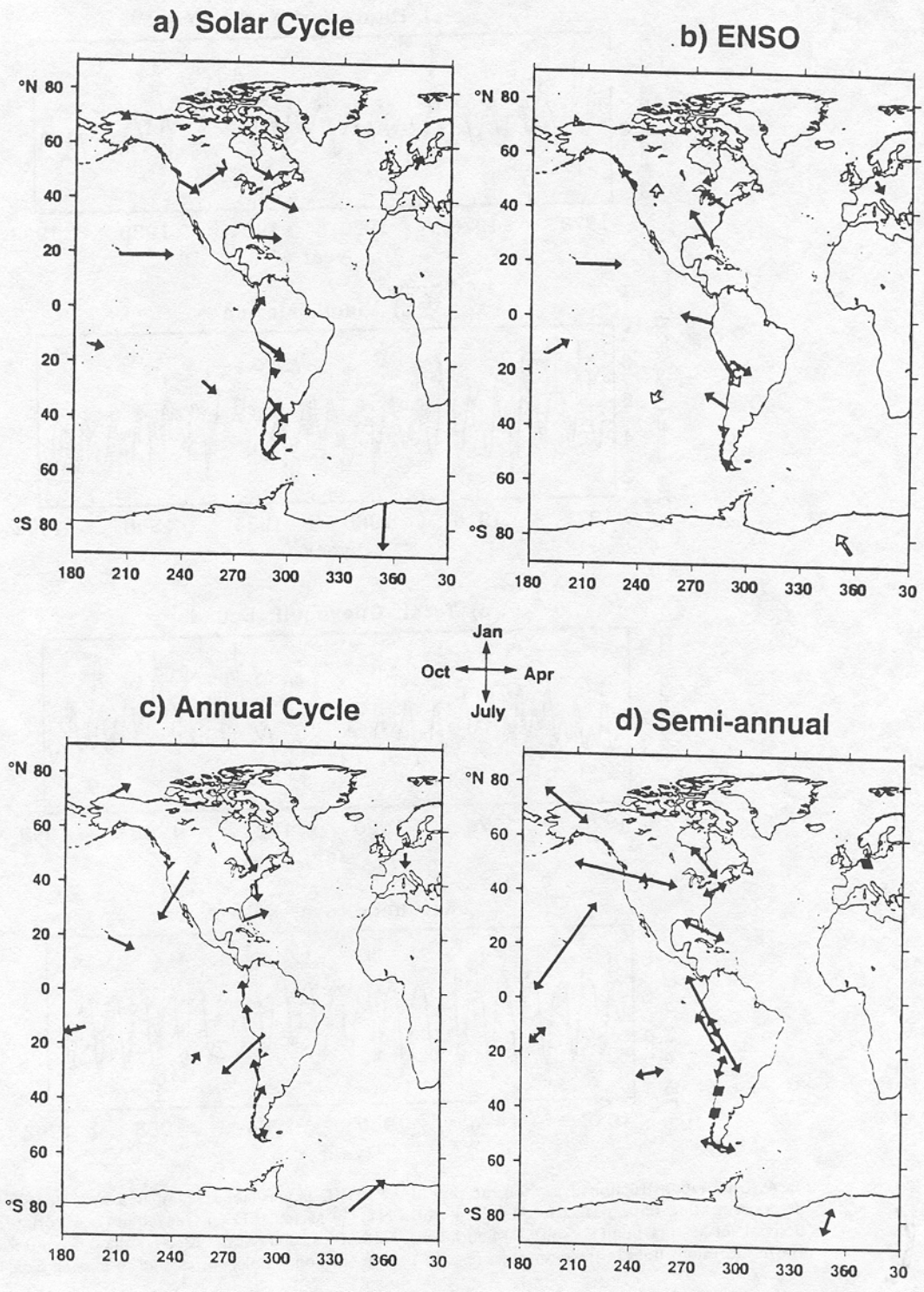

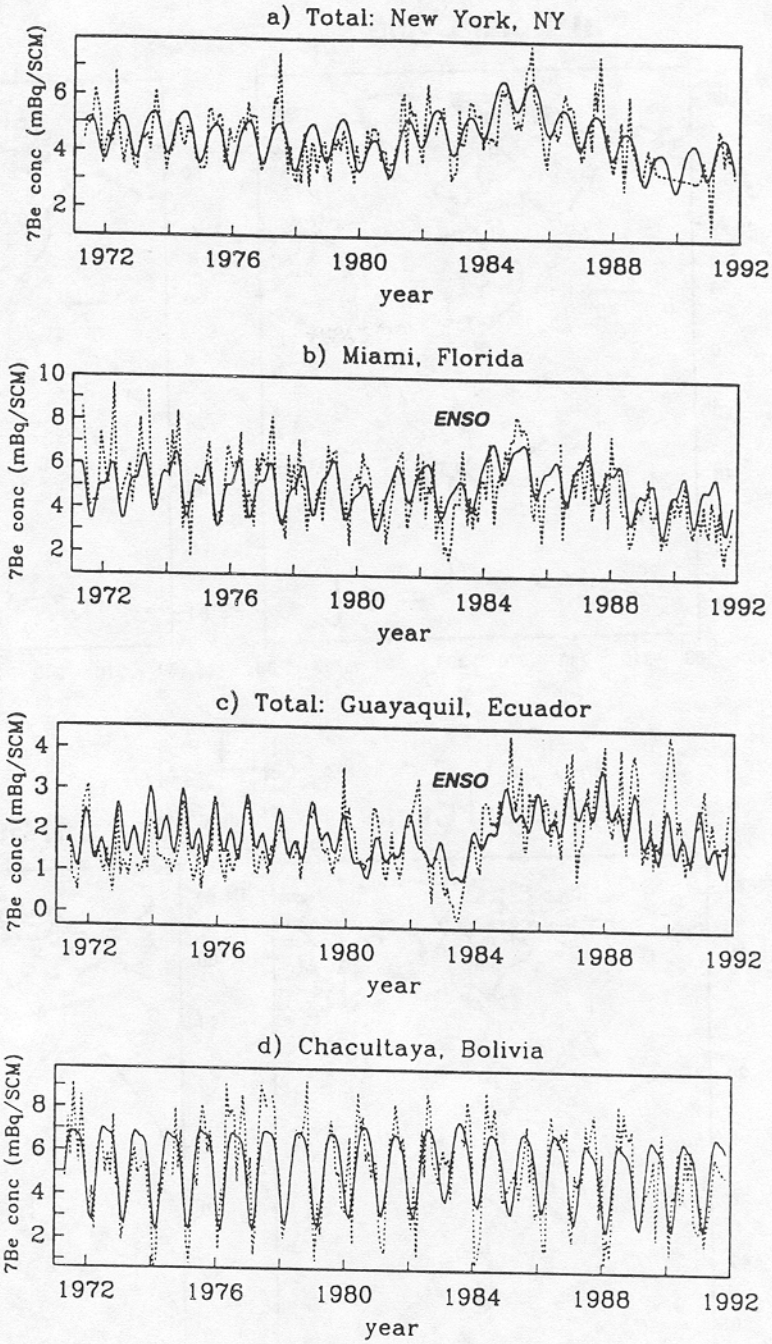

Fig. 4. Total reconstructions based on the sum of the 4 SVD modes (solid), compared with monthly average raw ^{7}Be concentration data (dashed) at: (a) New York, NY; (b) Miami, FL; (c) Guayaquil (Ecuador); (d) Chacultaya (Bolivia); (e) Mauna Loa (Hawaii); (f) South Pole. Note the different scales used for the different series. Units are mBq/m^3. Straight lines in the data series (e.g., in 1985 at the South Pole) correspond to missing data.

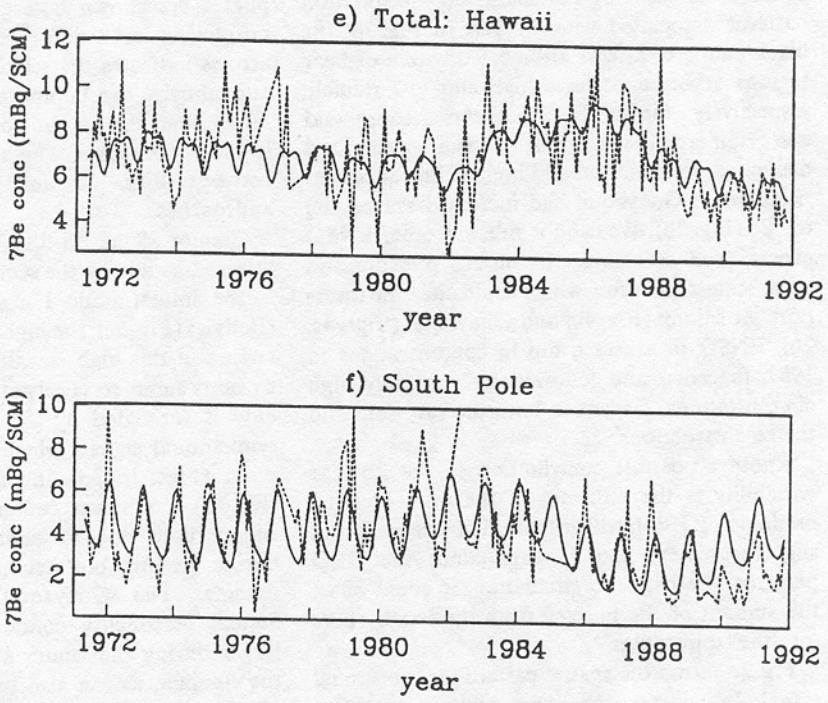

Table 1. *Percent variance explained by SVD modes at the 6 sites shown in Fig. 4*

Site	Solar	ENSO	Annual	Semi-annual	Total
New York, NY	25.2	2.9	18.4	0.5	47.0%
Miami, FL	8.0	3.9	18.1	4.7	34.7%
Guayaquil, Ecuador	12.4	4.0	7.4	8.4	32.2%
Chacultaya, Bolivia	0.8	0.4	35.7	2.5	39.4%
Mauna Loa, Hawaii	13.6	1.3	3.4	0.8	19.1%
South Pole	14.3	0.4	27.9	1.3	32.8%

cycle, are able to penetrate near the poles and enhance ^{7}Be production there, while the magnetic field shields the rest of the atmosphere (Lal and Peters, 1967). Among the sites where we have calculated the total reconstructions (sum of 4 modes), New York (Fig. 4a), Guayaquil (4c), Hawaii (4e), and the South Pole (4f) show the solar cycle influence most clearly, both in the reconstructions and in the raw data. There is no apparent explanation for the relatively small influence of the solar cycle at Chacultaya (4d) and Miami (4b).

In Fig. 2b, we show the $\approx$2.5 year mode at Mauna Loa and Guayaquil, where this mode explains 1.3% and 4.0% of the observed variability, respectively. We infer this to be an "ENSO" (El Niño/Southern Oscillation) signal, both because its frequency falls within the characteristic 2–7 year ENSO band (Mann and Park, 1994), and because of its notable strength during the large 1982–1984 ENSO event. Presumably other ENSO events during the time of study are less evident because the strongest event also dominates in the frequency domain, so that other events having slightly different characteristic frequencies would not contribute to the 2.5-year mode. Fig. 3b shows the spatial patterns for the variability. We expect ^{7}Be, as an aerosol-borne species, to be

primarily affected by the change in precipitation patterns associated with ENSO. In Fig. 3b, the black and gray arrows are located within or near regions expected to have high and low rainfall, respectively, during ENSO events (Ropelewski and Halpert, 1987). Thus, Hawaii experienced decreased precipitation and higher ^{7}Be concentrations, while Guayaquil had increased scavenging of ^{7}Be (Fig. 2b). We cannot rule out other ENSO effects, such as changes in surface pressure and large-scale circulation, which could alter ^{7}Be transport. At Miami (Fig. 4b) and Guayaquil (Figs. 4c, 2b), ENSO produces a dip in concentrations in 1983, preceded and followed by unusually high concentrations, evident in both the raw data and the reconstructions.

Another possible contribution to the 2.5-year variability is the influence of the quasi-biennial oscillation (QBO), which typically has a period of slightly greater than 2 years. Since the QBO perturbs stratospheric circulation, it could affect the amount of ^{7}Be injected from the stratosphere into the troposphere.

Fig. 3c shows the spatial pattern for the annual signal. In general, maximum concentrations at continental sites occur during the summer months; thus, the arrows in the northern and southern hemispheres point in opposite directions (an exception, Chacultaya (Bolivia) is discussed below). Over continents, convective activity, both with and without precipitation, is most active during the summers. It therefore appears that the subsidence associated with convection is the dominant mechanism for carrying ^{7}Be to the surface. Note that the high-elevation sites have higher amplitude annual signals. Precipitation patterns also contribute to the annual variability, particularly in the tropics and sub-tropics. In Miami, for example, relatively low precipitation in the spring accounts for the maximum springtime concentrations. In the Arctic, sites such as Barrow, Alaska (Fig. 3c), have ^{7}Be seasonality that is generated by a combination of lateral ^{7}Be transport from lower latitudes during the winter, increased subsidence in the spring (Dibb et al., 1994), and higher precipitation during the summer (Schutz and Gates, 1971, 1972, 1973, 1974).

These trends are also evident in a study using a larger data set, including those used in the SVD analysis, in which we fit a sine-curve to the average annual seasonality at each site. The sinusoid phases are shown in Fig. 5. For this figure, we normalized each data record, so the size of the arrows indicates the relative degree to which the annual cycle can be approximated by a sinusoid, rather than the amount of variance explained as in the SVD figures. The agreement of the phases between Figs. 3c and 5 substantiates both approaches.

Greater detail in the seasonal variability is attained by adding the semi-annual mode (Fig. 3c) to the annual mode. For example, at Chacultaya (Bolivia) (Fig. 2c), the high concentrations characteristic of this high elevation site are punctuated by rainy summers (Feely et al., 1988). This seasonality is simulated by the combined annual and semi-annual signals which are nearly 90° out of phase (Figs. 3c, 3d). In contrast, the South Pole (Fig. 4f) has sharp concentration peaks in the summertime due to enhanced vertical mixing during the brief polar summer, and broad winter minima. The Guayaquil (Ecuador) (Fig. 2d) annual seasonality contains double peaks, the larger during the winter and the smaller during the summer, as can also be seen in the raw data (Fig. 4c). Here, the concentration correlates with precipitation, since highest rainfall is during the winter and a lesser peak occurs during the summer (Schutz and Gates, 1971, 1972, 1973, 1974). Thus, it appears that convective subsidence associated with the precipitation delivers more ^{7}Be to the surface than the precipitation scavenges. Double peaking is also observed at Miami (Fig. 4b). New York (Fig. 4a) has a nearly pure sinusoidal annual signal, with little contribution from the semi-annual variability. New York's seasonality is mostly affected by the enhanced vertical convective mixing during the summer, since precipitation is relatively constant throughout the year.

3. Conclusions

The SVD method has helped to distinguish the relative contributions of a few processes to the variability of ^{7}Be surface air concentrations. Fig. 4 and Table 1 indicate that up to 47% of monthly ^{7}Be concentration variability can be explained by the 4 modes, corresponding to the solar cycle, ENSO, the annual cycle and the semi-annual signals. In the SVD approach, maximum variability is captured because the phase of the signals is

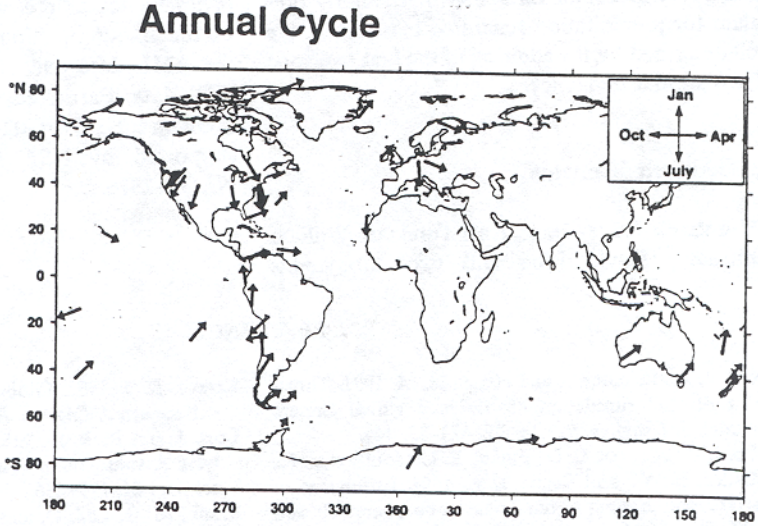

Fig. 5. The annual cycle maxima for a larger data set found by fitting a sinusoid to the normalized average seasonal records. Data are from Kolb (1992) (Norway and Germany), Turekian and Graustein (unpublished data) (Mace Head, Bermuda, Izania, Barbados, New Haven, Santa Rosa, Champaigne), Dibb et al. (1994) (Alert, Canada), and the remainder are from the Environmental Measurements Laboratory (referenced in the Introduction).

permitted to vary spatially. This approach shows the degree to which different locations are affected by different mechanisms. Without the aid of the SVD, simple global patterns for ^{7}Be variability are not apparent.

The results of an SVD study can contribute to the interpretation of modeling studies. The SVD helps distinguish between short-term effects in the observations, which lie within the time-scales of GCM studies, and longer-term trends which a short term (e.g., single year) GCM study cannot simulate. For the case of ^{7}Be, it is helpful to isolate the semi-annual and annual effects, which should be reproduced in models such as those used in Brost et al. (1991). The model, in turn, may then be used to help determine the cause of the annual and semi-annual patterns. The magnitude of the longer-term effects, such as the solar cycle and ENSO, can be assessed using the SVD, and can be used to improve the methods of comparing model output with data.

Eleven-year variability probably results from the influence of the solar cycle on ^{7}Be production. This is confirmed by the anticorrelation between the 11-year mode and the solar cycle (Fig. 2a), and because of the reasonably good global spatial coherence (Fig. 3a). The solar-cycle effects can be quite large, explaining, for example, 25% of the total variability at New York (Table 1). The solar-cycle effect is significant enough that data should be corrected before comparing with model output that has used a source corresponding to a particular solar activity. Although the SVD does produce the expected anti-correlation between ^{7}Be concentrations and solar activity, we have found no correlation between the effect of the solar cycle and proximity to the regions of high ^{7}Be production, namely high altitude and high latitude locations. The South Pole station has responded differently from the other locations, and has highest concentrations during the descending limb of a solar maximum. It thus appears that particles associated with solar activity are able to penetrate near the pole, while such low-energy particles are shielded by the magnetic field elsewhere.

The major effect of ENSO on ^{7}Be concentrations corresponds to changes in precipitation patterns. Without the SVD, it would have been difficult to attribute the resulting relatively small fluctuations in the data to ENSO.

We constructed seasonal variability from the sum of the annual and semi-annual modes. The analysis confirms a general trend toward summer seasonal maxima in ^{7}Be concentrations over continents, as is expected to result from increased convective activity during the summer. Departures

from pure sinusoidal variability, particularly prevalent for precipitation-generated seasonality, are well described by the addition of the first overtone of the annual frequency.

4. Acknowledgements

We thank Jeffrey Park, Karl Turekian, William Graustein, David Rind and two anonymous reviewers for helpful discussions and comments on the manuscript. John Kada provided copies of the EML data and H. Wershofen provided the PTB data. Partial support for D. Koch is from DOE grant DE-FG02–94ER61925. M. Mann is supported by NSF grant ATM-9222591 and NAG5–2316.

REFERENCES

Brost, R. A., Feichter, J. and Heimann, M. 1991. Three-dimensional simulation of ^{7}Be in a global climate model. *J. Geophys. Res.* **96**, 22, 423–22, 445.

Dibb, J. E., Meeker, L. D., Finkel, R. C., Southon, J. R., Caffee, M. W. and Barrie, L. A. 1994. Estimation of stratospheric input to the Arctic troposphere: ^{7}Be and ^{10}Be in aerosols at Alert, Canada. *J. Geophys. Res.* **99**, 12, 855–12, 864.

Feely, H. W., Toonkel, L. and Larsen, R. J. 1981. Radionuclides and trace elements in surface air. In: *Rep. EML-395*, Environmental Measurements Laboratory, US Dept. of Energy, New York.

Feely, H. W., Larsen, R. J. and Sanderson, C. G. 1985. Annual report of the surface air sampling program. In: *Rep. EML-440*, Environmental Measurements Laboratory, US Dept. of Energy, New York.

Feely, H. W., Larsen, R. J. and Sanderson, C. G. 1988. Annual report of the surface air sampling program. In: *Rep. EML-497*, Environmental Measurements Laboratory, US Dept. of Energy, New York.

Hötzl, H., Rosner, G. and Winkler, R. 1991. Correlation of ^{7}Be concentrations in surface air and precipitation with the solar cycle. *Naturwissenschaften* **78**, 215–217.

Kolb, W. 1992 Aktivitatskonzentrationen von radionukliden in der bodennahen luft norddeutschlands und nordnorwegens im zeitraum von 1963 bis 1990. In: *PTB-Bericht Ra-29*, Phys.-Tech. Bundesanst., Braunschweig, Germany.

Lal, D. and Peters, B. 1967. Cosmic ray produced radioactivity on the Earth. *Hand. Phys* **46**, 551–612.

Larsen, R. J. and Sanderson, C. G. 1990. Annual report of the surface air sampling program. In: *Rep. EML-524*, Environmental Measurements Laboratory, US Dept. of Energy, New York.

Larsen, R. J. and Sanderson, C. G. 1991. Annual report of the surface air sampling program. In: *Rep. EML-541*, Environmental Measurements Laboratory, US Dept. of Energy, New York.

Larsen, R. J. 1993. Global decrease of Beryllium-7 in surface air. *J. Environ. Radioactivity* **18**, 85–87.

Lees, J. and Park, J. 1995. Multiple-taper spectral analysis: A stand-alone C-subroutine. *Computers & Geosciences* **21**, 199–236.

Mann, M. E., Lall, U. and Saltzman, B. 1995. Decadal-to-centennial-scale climate variability: Insights into the rise and fall of the Great Salt Lake. *Geophys. Res. Lett* **22**, 937–940.

Mann, M. E. and Park, J. 1994. Global-scale modes of surface temperature variability on interannual to century timescales. *J. Geophys. Res.* **99**, 25, 819–25, 833.

O'Brien, K., De La Zerda Lerner, A., Shea, M. A. and Smart, D. F. 1991. The production of cosmogenic isotopes in the Earth's atmosphere and their inventories. In: *The sun in time*. University of Arizona Press, 317–342.

Percival, D. B. and Walden, A. T., 1993. In: *Spectral analysis for physical applications*. Cambridge University Press, Cambridge.

Ropelewski, C. F. and Halpert, M. S. 1987. Global and regional scale precipitation patterns associated with the El Niño/Southern Oscillation. *Monthly Weather Review*. **115**, 1606–1626.

Schutz, C. and Gates, W. L. 1971. *Global climatic data for surface, 800 mb, 400 mb: January*. The Rand Corporation, R-915-ARPA, November.

Schutz, C. and Gates, W. L. 1972. *Global climatic data for surface, 800 mb, 400 mb: July*. The Rand Corporation, R-1029-ARPA, November.

Schutz, C. and Gates, W. L. 1973. *Global climatic data for surface, 800 mb, 400 mb: April*. The Rand Corporation. R-1317-ARPA, December.

Schutz, C. and Gates, W. L. Global 1974. *Climatic data for surface, 800 mb, 400 mb: October*. The Rand Corporation. R-1425-ARPA, March.

Thomson, D. J. 1982. Spectrum estimation and harmonic analysis. *IEEE Proc.* **70**, 1055–1096.